

# **Seasonal variability of mixed layer in the central Arabian Sea and its implication on nutrients and primary productivity**

S. Prasanna Kumar and Jayu Narvekar

National Institute of Oceanography, Dona Paula, Goa-403 004, India.

---

## **Abstract**

The upper layers of the ocean play an important role in the regulation of the ocean-atmosphere as a coupled system. The Arabian Sea, situated in the western part of the northern Indian Ocean, participates in the intense air-sea exchange processes associated with the semi-annually reversing monsoons. During winter monsoon the weak northeast trade wind brings cool, dry continental air while during the summer monsoon the strong southwest wind brings humid maritime air into the Arabian Sea. It is natural to expect that these semiannual atmospheric forcing would modulate the thickness of the upper ocean. The seasonal variability of the mixed layer in the central Arabian Sea (equator to 25°N and 62°E to 66°) was studied using hydrographic data from NODC and INODC, while atmospheric forcing responsible for the observed changes were explored using meteorological data from COADS and FSU winds. The mixed layer depth (MLD) and sea surface temperature (SST) in the central Arabian Sea, to a large extent was regulated by the incoming solar radiation and wind forcing. The Ekman dynamics associated with the Findlater Jet controlled the mixed layer depth during summer monsoon, while in winter the cooling and convective mixing regulated the MLD. We speculate that the deep mixed layer during February-March in the southern region is associated with that of the Rossby wave propagation. During spring and fall Intermonsoons, the weak winds along with strong incoming solar radiation lead to the formation of thin, warm and stratified mixed layer. We show that biological productivity of the Arabian Sea is rigidly coupled to the seasonal cycle of MLD, which regulates the nutrient levels in the euphotic zone.

## 1. Introduction

The upper layers of the ocean play an important role in the exchange of energy and mass between the atmosphere and the underlying ocean. It is through this layer that the atmosphere feels the ocean and hence the changes within this layer will regulate the ocean-atmosphere as a coupled system. Apart from this, bulk of the biological productivity of the World Oceans critically depends on the physical and chemical changes taking place within this layer. The ocean surface mixed layer owes its high degree of vertical uniformity to mixing caused by turbulence. Atmospherically driven forcing that regulates mixing in the upper ocean are winds, waves, solar heating, evaporation and precipitation (Fig.1). Since the atmospheric forcing are highly variable on space-time scales, the geographical location, to a great extent, decides the structure and variability of the upper mixed layer. The Arabian Sea, situated in the western part of the northern Indian Ocean, participates in the intense air-sea exchange processes associated with the semi-annually reversing monsoon system. During winter (northeast) monsoon (November-February), the weak ( $\sim 5$  m/s) northeast trade wind brings cool, dry continental air while during the summer (southwest) monsoon (June-September) the strong ( $\sim 15$  m/s) southwest wind brings humid maritime air into the Arabian Sea. Consistent with the wind reversal, the surface circulation of the basin also undergoes seasonal change. It is natural to expect that these semiannual atmospheric forcing would modulate the thickness of the upper ocean by altering the thermal and mechanical inertia of the layer. Several studies in the past attempted to understand the changes in the mixed layer in the Indian Ocean including the Arabian Sea either based on individual cruises (e.g., Molinari et al., 1986; Rao, 1986;

Gopalakrishna et al., 1988) or climatology (e.g., Rao et al., 1989; Monterey and Levitus, 1997). These studies attributed the changes in the mixed layer to the wind-mixing and/or net heat flux. Recent model studies, however, indicated the possible role of remote forcing (Perigaud and Delecluse, 1992; McCreary et al., 1993) in influencing the dynamics of the Arabian Sea. In the present study, we analyzed the seasonal variability of mixed layer in the central Arabian Sea using more extensive and recent data from Indian research vessels and explored the atmospheric forcing in mediating such changes including the remote forcing. We chose central Arabian Sea to eliminate the direct effect of boundary processes such as coastal upwelling, boundary current etc.

## **2. Data and method**

In order to address the spatio-temporal variability of the mixed layer and the factors responsible for that, both the water column (hydrographic) data as well as the atmospheric data from various sources were utilized.

### ***2.1 Hydrographic Data***

The hydrographic data used for the study was mainly extracted from the National Oceanographic Data Center (NODC), CD-ROM, which contains temperature and salinity data from hydro cast as well as conductivity-temperature-depth (CTD) casts for the period 1900-1992 (Levitus et al., 1994). In addition, data was also used from the Indian Oceanographic Data Center (INODC), which contains hydro cast and CTD data, for the period 1976-1997, collected by the Indian research vessels. A preliminary examination of the data distribution in the Arabian Sea revealed that region

between longitude 62°E to 66°E has reasonably good spatio-temporal coverage. Hence the region encompassing equator to 25° N and 62°E to 66°E has been selected for this study (Fig. 2). In all a total of 1088 profiles of temperature and salinity were extracted from the above sources. Following quality control procedures were applied to obtain quality data.

At first, duplicate profiles as well as those with obvious errors were excluded by visual inspection. Then, profiles with depth less than 100m were eliminated, as mixed layer in the central Arabian Sea is normally encountered in the top 100m. These quality control procedures reduced the data set to 1015 profiles. Of this 748 profiles were obtained from hydro cast while 267 profiles were obtained from CTD cast. From the data distribution, it was evident that to obtain a monthly mean coverage it is necessary to prepare spatial mean profiles on 2° latitude and 4° longitude grids. Table 1 gives the number of profiles on each of the 2° x 4° grid. Based on these profiles monthly mean climatology of temperature and salinity were prepared on a 2° x 4° grids up to a depth of 500m. Monthly mean temperature and salinity data were used to calculate the sigma-t values (UNESCO, 1981).

We also used nitrate, chlorophyll *a* and primary productivity data in the upper 120m water column collected under the Indian JGOFS program during spring Intermonsoon (April-May, 1994), winter (February-March, 1995) and summer (July-August, 1995 & August 1996) monsoons (for details see Prasanna Kumar et al, 2000a).

## ***2.2 Atmospheric Data***

Atmospheric data used in the study has been derived from two sources. To derive incoming short wave radiation and evaporation, Comprehensive

Ocean Atmosphere Data Set (COADS) (Woodruff et al., 1987) was used which contains the monthly mean climatology of the surface meteorological observations on a  $2^{\circ} \times 2^{\circ}$  grid for the period 1950-1979. The monthly mean precipitation data on a  $2^{\circ} \times 2^{\circ}$  grid generated from the Very High Resolution Radiometer (VHRR) onboard the Indian National Satellite (INSAT) (see Ramesh Kumar and Prasad, 1996 for detail). For the computation of wind-stress curl, Florida State University (FSU) winds for the period 1993-97 on a  $1^{\circ} \times 1^{\circ}$  grid was used.

### **3. Criteria for selecting the mixed layer depth**

In applying the concept of mixed layer to an oceanic situation one must be careful to choose a mixed layer definition that matches the physics of the problem being studied. Operationally this is the depth at which some property has changed by specific amount from its surface value. Two types of mixed layer depth definitions have been most commonly used, the first is based on specifying a difference in temperature or density from the surface value (Wyrki, 1964 ; Levitus, 1982 ; Schneider and Muller, 1990). A second type of criteria is based on specifying a gradient in temperature or density (Bathen, 1972 ; Lukas and Lindstrom, 1991).

In order to decide what criteria should be followed to define mixed layer, it is important to examine the distribution of (physical) properties within the upper layer. Since the Arabian Sea undergoes seasonal, distribution of properties needs to be examined in space as well as in time. Winter and summer monsoons being the two prominent seasons, the vertical profiles of temperature, salinity and sigma-t for the month of January (peak of winter) and July (peak of summer) are presented for various grids (Fig.3). An

analysis of the profiles indicates that the isothermal, isohaline and isopycnal layer, in general, seems to coincide in the upper ocean irrespective of the season or location in the central Arabian Sea. Hence, in the present study we defined MLD as the depth at which the temperature is 1°C less than the surface value. For this purpose, the monthly mean temperature, salinity and sigma-t profiles were interpolated into 1m-depth interval using the cubic spline method.

#### **4. Results**

We begin with the analysis of the variation of monthly mean climatology of mixed layer depth (MLD) along with the sea surface temperature (SST) and salinity (SSS).

Time-latitude plot of mixed layer depth (Fig.4) showed deep mixed layer (>80m) during January-February in the region north of 15°N, while a second region of deep MLD was noticed between 3 and 6°N which persisted till March. From March and until May, MLD showed a decreasing trend attaining its shallowest (~30m) depth in April, and north of 23°N MLD was still shallow at around 20m. Once again during June to October, MLD showed a deepening trend in the region south of 17°N attaining the deepest value of >100m in July. In the north, however, MLD showed a steady decrease with latitude during this period. During October-November MLD once again decreased and subsequently showed an increasing trend in the north, north of 15°N, in December.

SST showed colder SST (<25.5°C) during January and February in the north, (>15°N) while southern region exhibited warmer SST with values up to 29°C (Fig.5). From March and until June, SST steadily increased attaining

its peak value of 30°C in May. During July to September, the Arabian Sea north of 11°N cooled by about 3.5°C, while only a marginal cooling was noticed in the southern region. A secondary warm SST was encountered in October (>27.5°C) followed by a cooling trend in November in the northern region, which continues till February.

Sea surface salinity (SSS) in the north, north of 15°N, was 36.4 psu during November and increased to 36.6 psu in December (Fig.6). During January and February surface salinity of 36.4 psu extended up to 13°N and showed a steady southward extension with time reaching up to 5°N in October. Interestingly, north of 19°N surface salinity was most of the time greater than 36.4 psu. Equatorial region, however, showed low salinity of about 35.0 psu.

Thus, the deep MLD during January and February in the north was associated with cold SST and high salinity, while that near the equatorial region was associated with warm SST and low salinity. Though shallow MLD during March-April and October coincided with warm SST, surface salinity distribution did not show any specific trend during this period. Similarly, the deeper MLD south of 16°N and progressively decreasing MLD towards the north during June to September did not show any corresponding co-variation either in SST or in SSS distribution. In order to understand this, we analyzed the physical forcing that regulates MLD such as incoming short wave radiation, wind and evaporation-precipitation (E-P).

The incoming short wave radiation exhibited a distinct biannual cycle in the central Arabian Sea (Fig.7). The primary heating in this region was from March to June with a peak in April-May (320 W/m<sup>2</sup>), corresponding to Spring intermonsoon, in the northern part. However, south of 10°N the peak occurred during March-April (300 W/m<sup>2</sup>). The secondary heating was seen

during September-October, corresponding to fall intermonsoon, with a peak value of  $240 \text{ W/m}^2$ . During the summer and winter monsoon periods the incoming short wave radiation reduced by  $100 \text{ W/m}^2$  and  $120 \text{ W/m}^2$  respectively from the spring intermonsoon value. The observed seasonal variability in SST appeared consistent with the changes in the incoming short wave radiation.

The wind speed, which was  $\sim 7 \text{ m/s}$  in January, decreased gradually to  $5 \text{ m/s}$  in March-April (Fig.8a). From May it increased rapidly peaking to  $13 \text{ m/s}$  in July and then decreased to about  $6 \text{ m/s}$  in October-November. Again in December wind speed was  $7 \text{ m/s}$ . The observed wind speed pattern though explained the cold SST during summer and shallow MLD during spring and fall intermonsoons, could not fully explain the MLD variations, especially during summer and winter in the northern latitudes. A look at the wind stress curl revealed negative values during June to September in the region south of  $17^\circ\text{N}$  and also north of  $21^\circ\text{N}$  during July to December (Fig.8b). However, between  $17^\circ\text{N}$  and  $21^\circ\text{N}$  wind stress curl showed positive values during June to September. This positive wind stress curl would drive an upward Ekman pumping and upwelling which in turn would lead to shoaling of mixed layer, as was seen in the MLD north of  $17^\circ\text{N}$ . Similarly the negative wind stress curl south of  $17^\circ\text{N}$  would induce downward Ekman Pumping and downwelling resulting in deep mixed layer. However, the positive wind-stress curl north of  $21^\circ\text{N}$ , during January and February and observed deep MLD still remains intriguing. This may point to the fact that the deep MLD may actually be the manifestation of latent-heat forcing on sea surface rather than the above mechanical forcing related with Ekman dynamics and could be explained in the light of E-P.



The E-P distribution revealed two periods of high evaporation, one during June-July and the other during December to February (Fig.9) in the northern part of the central Arabian Sea. The high evaporation during winter in the northern part leads to cooling as well as increase in salinity; both combined leads to densification of the upper layer waters and mixed layer deepening through convection. The negative E-P explains the observed low salinity in the equatorial region.

In order to explore the implication of mixed layer variability on the nutrients and the biological productivity we used the nitrate, chlorophyll *a* and primary productivity data. Nitrate distribution during spring intermonsoon showed that the upper 40m was devoid of any detectable levels of nitrate, but below this nitrate levels showed steady increase (Fig.10a). In accordance with the nitrate distribution, the vertical chlorophyll *a* distribution showed very low values in the upper 40m, and showed increasing trend with a subsurface chlorophyll maximum (SCM with a value of  $0.4 \text{ mg/m}^3$ ) situated at around 60m depth (Fig.10b). Below SCM the chlorophyll values decreased due to light limitation. The column integrated (up to 120m) primary production (PP) were low and showed marginal variation from  $163 \text{ mg C m}^{-2} \text{ d}^{-1}$  at  $11^\circ\text{N}$  to  $310 \text{ mg C m}^{-2} \text{ d}^{-1}$  at  $21^\circ\text{N}$ . Comparison with the mixed layer depth indicated that, the warm and comparatively thin mixed layer ( $\sim 30\text{m}$ ) was oligotrophic supporting very less chlorophyll and biological production. However, as the nitrate levels increased with depth a SCM develops. But with further increase in nitrate with depth, chlorophyll and PP did not increase as light becomes limiting.

During the summer monsoon, the nitrate isopleths showed shoaling towards north, with  $1\mu\text{M}$  shoaling up to 20m at  $18^\circ\text{N}$  (Fig.11a) from 90m depth at  $11^\circ\text{N}$ . Beyond  $19^\circ\text{N}$  latitude the  $1\mu\text{M}$  nitrate isopleth once again

showed deepening trend. Consistent with this, the chlorophyll *a* distribution also showed an increase from 0.4mg/m<sup>3</sup> at 11°N up to 1.0mg/m<sup>3</sup> at 17°N (Fig.11b), followed by a decreasing trend reaching a value of 0.4mg/m<sup>3</sup> at 21°N. In general, chlorophyll was highest in the upper 30m, between 16-19°N where nitrate isopleth shoaled the most. The column integrated PP was much higher than the spring intermonsoon period. It increased from 770 mg C m<sup>-2</sup> d<sup>-1</sup> at 11°N to 1782 and 1029 mg C m<sup>-2</sup> d<sup>-1</sup> respectively at 15° and 17°N; and then decreased to 830 mg C m<sup>-2</sup> d<sup>-1</sup> at 19°N. Thus, the higher chlorophyll and PP resulted from the elevated nitrate levels in the upper layers.

In the winter monsoon, nitrate distribution showed the surfacing of 1μM and 2μM isopleth north of 15°N and 17°N respectively (Fig.12a). Further north, the surface nitrate levels were between 2 and 3μM. The chlorophyll *a* distribution showed elevated values in the upper 30m, with a maximum of 0.4 mg/m<sup>3</sup> between 15-16°N in the upper 40m (Fig.12b). The column integrated PP increased from 335 mg C m<sup>-2</sup> d<sup>-1</sup> at 11°N to 643 mg C m<sup>-2</sup> d<sup>-1</sup> at 21°N. The wintertime chlorophyll and PP in the south (for e.g. at 11°N) were in general comparable to the spring intermonsoon values but towards the north the former were much higher (more than double) than the latter.

## **5. Discussion**

The observed variability of the mixed layer depth in the central Arabian Sea clearly showed a strong seasonality which could be understood in the context of time varying atmospheric forcing such as incoming solar radiation, wind-stress curl and fresh water flux (E-P).

The incoming short wave radiation during winter (November-February) was about  $60 \text{ w/m}^2$  less than the fall intermonsoon (October) value. This reduction in the incoming short wave radiation must cool the Arabian Sea. In addition to this, the fresh water flux (E-P) showed high evaporation (in excess of  $100 \text{ mm/month}$ ), especially north of  $10^\circ\text{N}$ . These combined effects of reduced short wave radiation and enhanced evaporation, under the influence of northeasterly dry continental winds ( $4\text{-}5 \text{ m/s}$ ), cool the upper layers of the northern Arabian Sea as is evident by the cold SST ( $<25.5^\circ\text{C}$ ) north of  $15^\circ\text{N}$ . The enhanced evaporation not only cools the surface waters but also increases the upper layer salinity, which was in excess of  $36.4 \text{ psu}$  in the north. The combined cooling as well as increase in salinity increased the density of the surface waters of the northern Arabian Sea and initiates convection (Prasanna Kumar and Prasad, 1996; Prasanna Kumar et al., 2001). Winter convection, though common in the higher latitude is unique to the Arabian Sea, which is a tropical basin. Convective mixing slowly erodes the upper thermocline/nutracline and deepens the mixed layer ( $>80\text{m}$ ) as seen from the time evolution of MLD. Erosion of the nutracline elevates the nitrate levels in the mixed layer as was evident from the higher nitrate levels ( $1\text{-}2 \mu\text{M}$ ) in the surface waters in the northern latitudes. High nitrate concentration in the mixed layer lead to the observed high chlorophyll concentrations and primary production which was about twice higher than that seen in the region out side the winter cooling. The high mixed layer depth noticed between  $3$  and  $6^\circ\text{N}$  during February and March, however, could not be explained in the light of the above atmospheric forcing and calls for an alternate mechanism. This deep MLD appears to be associated with the propagating Rossby waves. In order to explore this, we used monthly mean sea surface height (SSH) anomalies derived from

TOPEX/Poseidon altimeter during 1993 to 1997. The sloping contours in the time-longitude plots of SSH anomalies along 5°N (Fig.13) indicate the signatures of westward propagating Rossby wave. Based on a comparison of the sea level anomaly and the zonal winds, Prasanna Kumar et al. (2000b) concluded that the westward propagation of sea level is independent of the seasonal reversal of zonal winds in the Arabian Sea.

During spring intermonsoon (March-May), when the incoming short wave radiation was maximum ( $320 \text{ w/m}^2$ ) the SST also peaked ( $30^\circ\text{C}$ ). The intense solar heating resulted in the highly stratified and shallow mixed layer ( $\sim 30\text{m}$ ) observed in April-May. The weak winds ( $\sim 5 \text{ m/s}$ ) prevalent during this time of the year, were unable to break the stratification and induce mixing of subsurface waters with the surface waters. As a result, the upper layer was devoid of any nutrients as could be seen from the nitrate distribution. Consistent with this, chlorophyll *a* distribution showed an oligotrophic mixed layer ( $< 0.05\text{mg/m}^3$ ). Below the mixed layer, as the nitrate concentrations increased with depth, a SCM was noticed at 60m ( $0.4\text{mg/m}^3$ ). However, the integrated chlorophyll and primary production was the least, one-half lesser than its winter monsoon values.

With the onset of summer (June-September), the incoming short wave radiation decreased by about  $100 \text{ w/m}^2$  from its peak spring intermonsoon value. At the same time the wind speed showed a 3-fold increase, from its spring intermonsoon value, which increased the evaporation ( $E-P > 100 \text{ mm/month}$ ). Thus, both increased wind speed and reduced solar insolation lead to the observed cold SST ( $\sim 26.5^\circ\text{C}$ ). The increased wind speed was associated with the low level Findlater Jet that becomes active over the Arabian Sea during this time of the year. The positive wind stress curl north of the Findlater Jet axis ( $\sim 17^\circ\text{N}$  along  $64^\circ\text{E}$ ) induced open ocean upwelling

(Bauer et al., 1991; Prasanna Kumar et al., 2001b) and resulted in shallow mixed layer (30-40m) as observed in the MLD distribution. Towards the south of the Findlater Jet axis open ocean down welling driven by negative wind stress curl gave rise to deep mixed layer (>80m). Associated with the shoaling of mixed layer, the nitracline also shoaled as is evident from the depth of  $1\mu\text{M}$  nitrate isopleth. The observed high chlorophyll a ( $>0.5$  and up to  $1\text{mg}/\text{m}^3$ ) between  $16-19^\circ\text{N}$  indicates the nitrate availability in the upper 30m. Though the high chlorophyll distribution could be explained in terms of upwelling of high nutrients from subsurface, the relatively high values in the southern part where down welling takes place needs other nutrient source. One such source could be advection of upwelled nutrient rich waters from Somalia into the central Arabian Sea as suggested by Prasanna Kumar et al. (2001b). In fact the observed high chlorophyll and PP results from the nutrient supply to the surface layers during summer monsoon through a combination of processes such as win-induced mixing, advection of nutrient rich waters from Somalia and Arabia upwelling, and the open ocean upwelling driven by Findlater Jet.

As the summer monsoon withdraws and fall intermonsoon sets in, which is the period of secondary heating, the incoming short wave radiation increases by about  $40\text{ w}/\text{m}^2$  from its summer value. The wind speed at this time reduces to its springtime value. Consistent with this the SST increases to more than  $27.5^\circ\text{C}$  and MLD shoals.

### **Acknowledgements**

We thank G.V. Reddy for extracting hydrography data and James N. Stricker for providing FSU winds. Jayu Narvekar acknowledges the financial support from CSIR. This is NIO contribution number 3990.

## References

- Bathen, K.H., 1972. On the seasonal changes in the depth of mixed layer in the north Pacific Ocean. *Journal of Geophysical Research* 77, 7138-7150.
- Bauer, S., Hitchcock, G. L, Olson, D. B., 1991. Influence of monsoonally forced Ekman dynamics of upper surface layer depth and phytoplankton biomass distribution in the Arabian Sea, *Deep Sea Research* 38 (Part A), 531-533.
- Gopalakrishna, V.V., Sadhuran, Y., Ramesh Babu, V., 1988. Variability of mixed layer depth in the northern Indian Ocean during 1977 and 1979 summer monsoon seasons, *Indian Journal of Marine Sciences* 17, 258-264.
- Levitus, S., 1982. *Climatological Atlas of the World Ocean*, NOAA Professional paper 13, National Oceanic and Atmospheric Administration, Rockville Md, 173 pp.
- Levitus, S., Gelfeld, R., Boyer, T., Johnson, D., 1994. Results of the NODC Oceanographic Data Archaeology and Rescue Projects, Key to Oceanographic Records Documentation No. 19, NODC, Washington, D.C., 73pp.
- Lukas, R., Lindstrom, E., 1991. The mixed layer of western equatorial Pacific Ocean. *Journal of Geophysical Research* 96, 3343-3357.
- McCreary, J.P., Kundu, P.K., Molinari, R.L., 1993. A numerical investigation of dynamics, thermodynamics and mixed-layer processes in the Indian Ocean. *Progress in Oceanography* 31, 181-244.
- Molinari, R.L., Swallow, J., Festa, J.F., 1986. Evolution of the near-surface thermal structure in the western Indian Ocean during FGGE 1979. *Journal of Marine Research* 44, 739-762.
- Monterey, G., Levitus, S., 1997. Seasonal variability of mixed layer depth for the world ocean, NOAA atlas NESDIS 14, U.S. Gov. Printing Office, Washington, D.C., 87 figures & 96pp.
- Perigaud, C., Delecluse, P., 1992. Annual sea level variations in the southern tropical Indian Ocean from geosat and shallow-water simulations. *Journal of Geophysical Research* 97, 20169-20178.
- Prasanna Kumar, S., Prasad, T.G., 1996. Winter cooling in the northern Arabian Sea. *Current Science* 71, 834-841.
- Prasanna Kumar, S., Madhupratap, M., Dileep Kumar, M., Gauns, M., Muraleedharan, P.M., Sarma, V.V.S.S., De Souza, S.N., 2000a. Physical control of primary productivity on seasonal scale in central and eastern Arabian Sea. *Proceedings of Indian Academy of Sciences (Earth and Planetary Science)* 109, 433-442.

- Prasanna Kumar, S., Unnikrishnan, A.S., Muraleedharan, P.M., 2000b. Signatures of Kelvin and Rossby wave propagation in the northern Indian Ocean from Topex/Poseidon altimeter. *Proceedings of PORSEC 1*, 276-279.
- Prasanna Kumar, S., Ramaiah, N., Gauns, M., Sarma, V.V.S.S., Muraleedharan, P.M., Raghukumar, S., Dileep Kumar, M., Madhupratap, M., 2001a. Physical forcing of biological productivity in the northern Arabian Sea during the northeast monsoon. *Deep-Sea Research II* 48, 1115-1126.
- Prasanna Kumar, S., Madhupratap, M., Dileep Kumar, M., Muraleedharan, P. M., De Souza, S. N., Mangesh, G. and Sarma, V. V. S. S., 2001b. High biological productivity in the central Arabian Sea during the summer monsoon driven by Ekman pumping and lateral advection. *Current Science* 81, 1633-1638.
- Ramesh Kumar, M.R., Prasad, T.G., 1996. Annual and interannual variations of precipitation over the tropical Indian Ocean. *Journal of Geophysical Research* 102, 18519-18527.
- Rao, R.R., 1986. Cooling and deepening of the mixed layer in the central Arabian Sea during Monsoon-77: Observations and simulations. *Deep-Sea Research* 33, 1413-1424.
- Rao, R.R., Molinari, R.L., Festa, J.F., 1989. Evolution of the climatological near-surface thermal structure of the tropical Indian Ocean. *Journal of Geophysical Research* 94, 1081-10815.
- Schneider, N., Muller, P., 1990. The meridional and seasonal structures of the mixed layer depth and its diurnal amplitude observed during the Hawaii-to-Tahiti Shuttle Experiment *Journal of Physical Oceanography* 20, 1395-1404.
- UNESCO, 1981. Technical papers in marine science. United Nations Educational, Scientific and Cultural Organization, Paris, 192pp.
- Woodruff, S. D., Slutz, R. J., Jenne, R. L., Sturmer, P. M., 1987. A comprehensive ocean-atmosphere data set, *Bulletin of the American Meteorological Society* 68, 1239-1250.
- Wyrtki, K., 1964. The thermal structure of the eastern Pacific Ocean, *Deutsche Hydrographische. Zeitschrift (Suppliment A8)*, 6-84.

Table 1. Number of temperature and salinity profiles in each of the 2° latitude (0-26 °N) x 4° longitude (62-66 °E) bin for each month.

Month	2° latitude x 4° longitude bin												
	0-2	2-4	4-6	6-8	8-10	10-12	12-14	14-16	16-18	18-20	20-22	22-24	24-26
<b>January</b>	9	6	3	5	2	3	2	3	5	4	5	5	4
<b>February</b>	4	8	7	5	3	4	3	16	5	22	54	19	7
<b>March</b>	2	1	2	2	5	3	3	3	8	6	15	18	10
<b>April</b>	4	7	6	3	12	5	6	12	3	3	7	10	2
<b>May</b>	12	11	8	8	8	14	6	56	8	9	12	10	11
<b>June</b>	4	5	14	7	4	6	4	56	10	2	7	1	-
<b>July</b>	4	2	6	2	11	9	11	2	4	4	4	-	-
<b>August</b>	24	9	8	12	13	5	7	21	10	11	8	3	-
<b>September</b>	-	5	6	1	6	3	-	2	6	7	6	-	4
<b>October</b>	-	-	1	1	2	2	2	9	4	9	5	3	1
<b>November</b>	-	-	-	-	7	2	8	1	1	3	3	4	2
<b>December</b>	-	-	1	1	3	6	3	8	4	11	7	1	-

The dash (–) line indicates no data.



## Legend to figures

Fig.1 Schematic representation of various forcing that is responsible for changes in the upper ocean mixed layer. The solar heating and precipitation stratifies and stabilizes the upper ocean while the wind, wave action and evaporation destabilizes it through mixing.

Fig.2 Location map of the study area in the Arabian Sea. The hatched rectangle (0-25°N, 62-66°E) indicates the region within which the data for the present study is analyzed.

Fig.3 Vertical profiles of temperature (dash-dot line), salinity (solid line) and sigma-t (broken line) for January (left) and July (right) for various 2-degree grids along 64°E.

Fig.4 Time-Latitude plot of mixed layer depth (MLD, m) along 64°E. The hatched region indicates MLD deeper than 80m .

Fig.5 Time-Latitude plot of sea surface temperature (SST, °C) along 64°E. The hatched region indicates SST colder than 25.5°C and 26.5°C during winter and summer respectively.

Fig.6 Time-Latitude plot of sea surface salinity (SSS, psu) along 64°E. The hatched region indicates salinity greater than 36.4 psu.

Fig.7 Time-Latitude plot of short wave radiation ( $\text{w/m}^2$ ) along 64°E.

Fig.8 Time-Latitude plot of (a) wind speed (m/s) and (b) wind-stress curl ( $\times 10^{-8}$  pascal  $\text{m}^{-1}$ ) along 64°E. Solid line at around 17°N during June to September represents the mean position of the axis of the Findlater Jet (see text for details).

Fig.9 Time-Latitude plot of E-P (mm/month) along 64°E. The stippled region shows where evaporation exceeds precipitation by 100 mm/month.

Fig.10 Vertical section of (a) nitrate ( $\mu\text{M}$ ) and (b) chlorophyll *a* ( $\text{mg/m}^3$ ) in the upper 120m depth during spring Inter monsoon (April-May 1994).

Fig.11 Vertical section of (a) nitrate ( $\mu\text{M}$ ) (b) and chlorophyll *a* ( $\text{mg}/\text{m}^3$ ) in the upper 120m depth during summer monsoon (August 1996). Note that data south of  $13^\circ\text{N}$  is from summer (July-August) 1995.

Fig.12 Vertical section of (a) nitrate ( $\mu\text{M}$ ) and (b) chlorophyll *a* ( $\text{mg}/\text{m}^3$ ) in the upper 120m depth during winter monsoon (February-March 1995).

Fig.13 Time-longitude plot of monthly mean (1993-97) SSH anomaly along  $5^\circ\text{N}$ . Shaded region indicates high sea level.

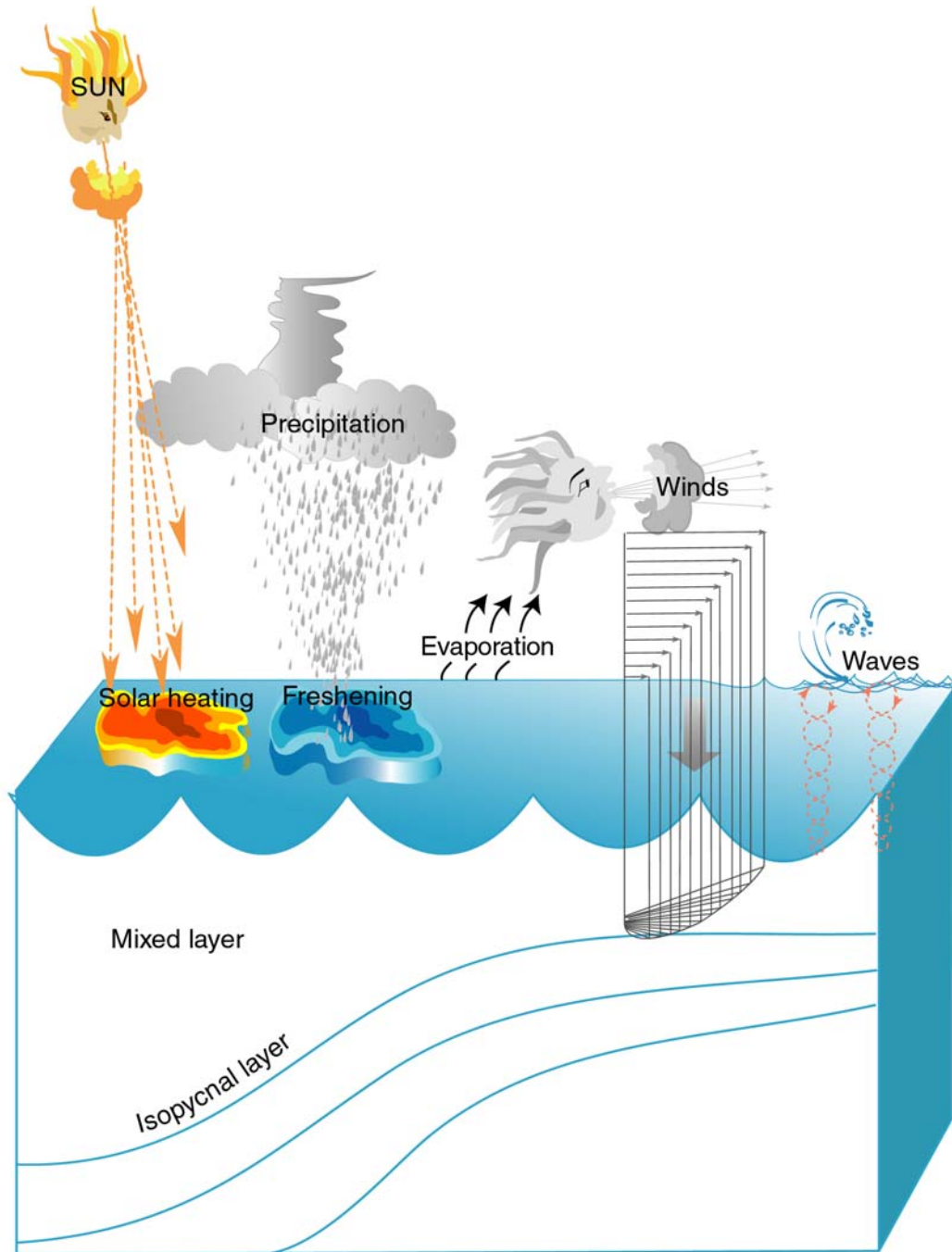


Fig.1 Schematic representation of various forcings that are responsible for changes in the upper ocean mixed layer. The solar heating and precipitation stratifies and stabilizes the upper ocean while the wind, wave action and evaporation destabilizes it through mixing.

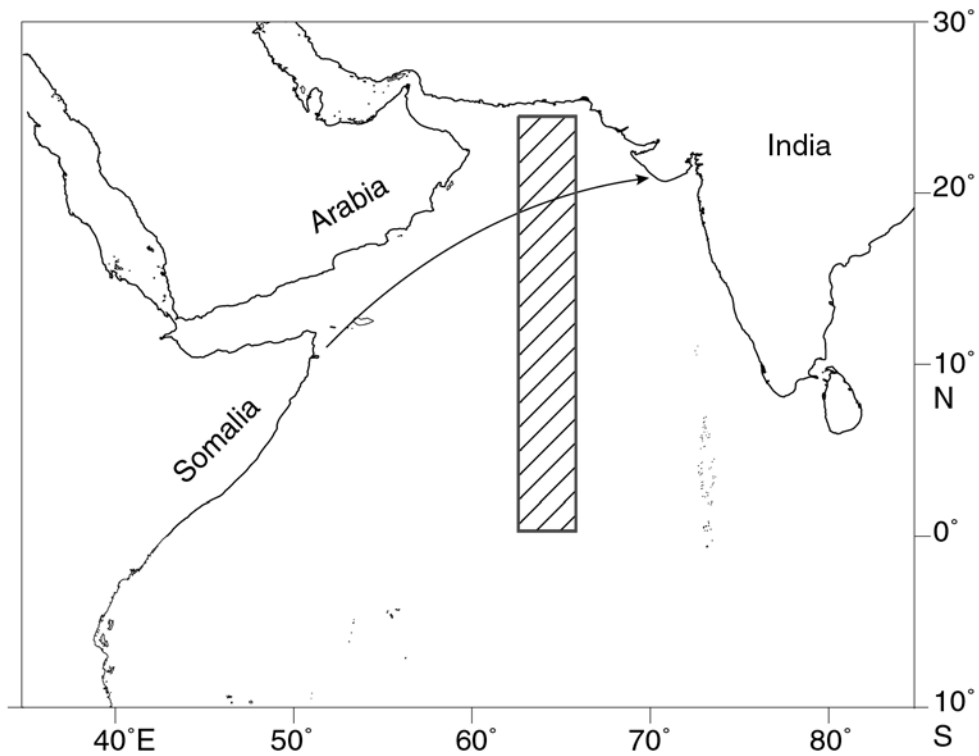


Fig.2 Location map of the study area in the Arabian Sea. The stippled rectangle (0-25°N, 62-66°E) indicates the region within which the data for the present study is analysed. The arrow indicates the position of the Findlater Jet axis.

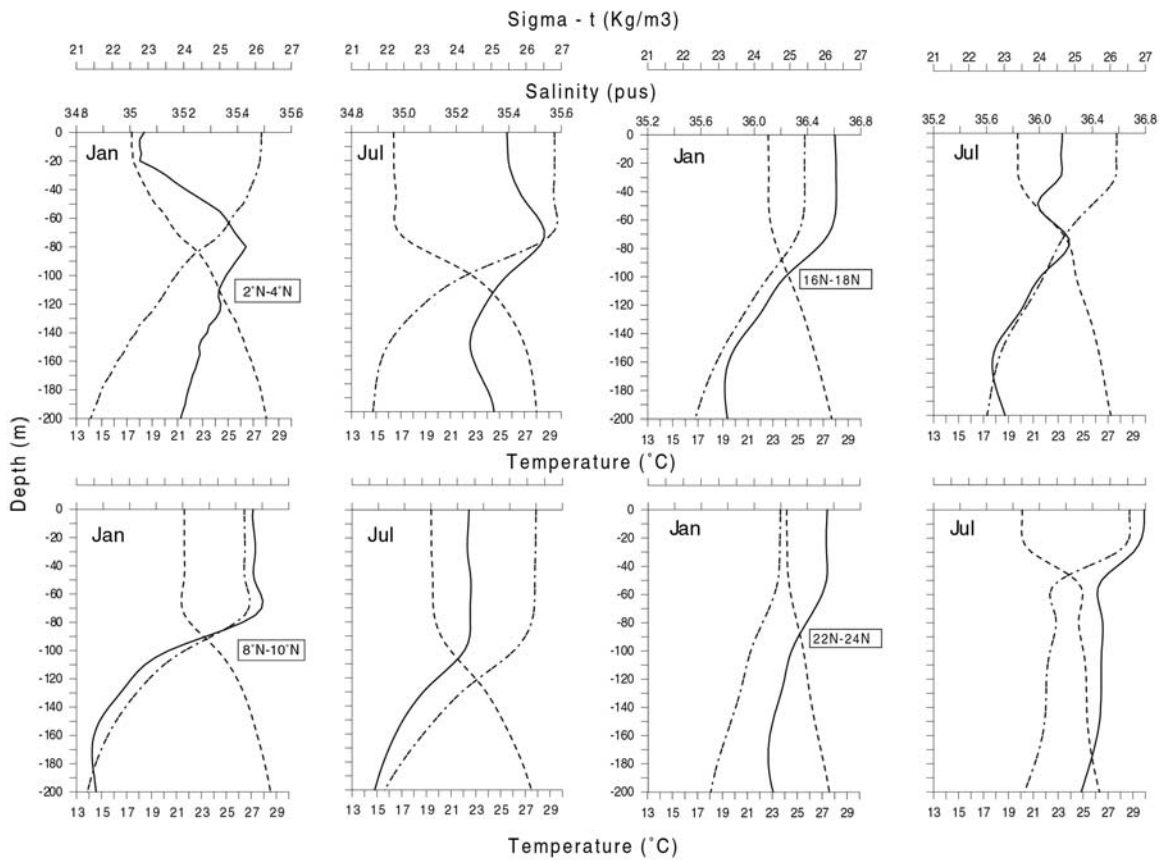


Fig.3 Vertical profiles of temperature (dash-dot line), salinity (solid line) and sigma-t (broken line) for January (left and July (right) for various 2-degree grids along 64°E.

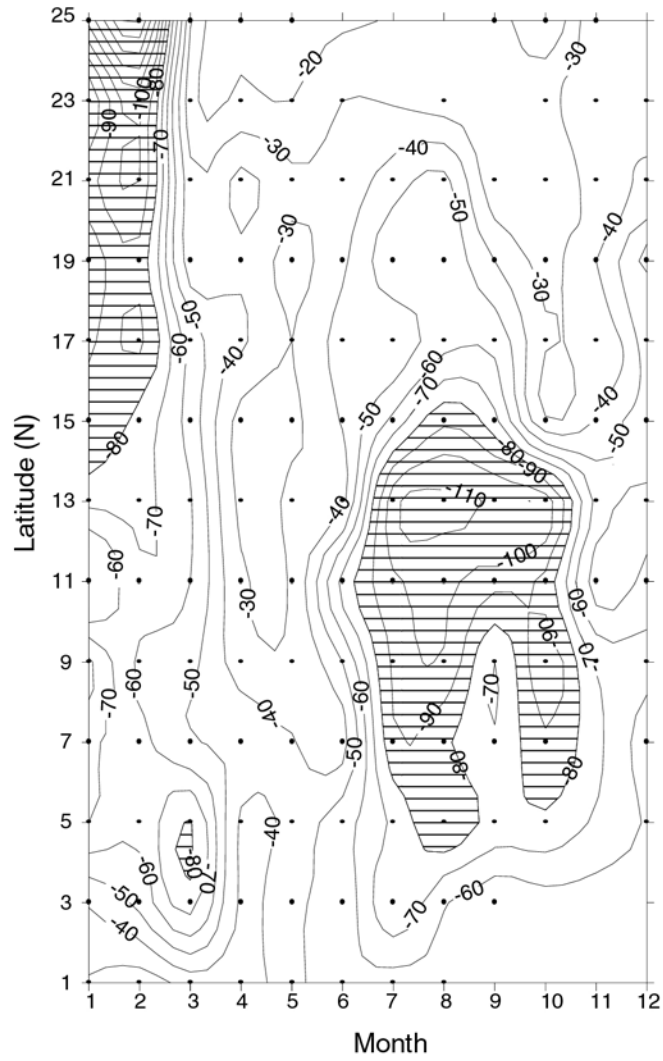


Fig.4 Time-Latitude plot of mixed layer depth (MLD, m) along 64°E. The hatched region indicates MLD deeper than 80m.

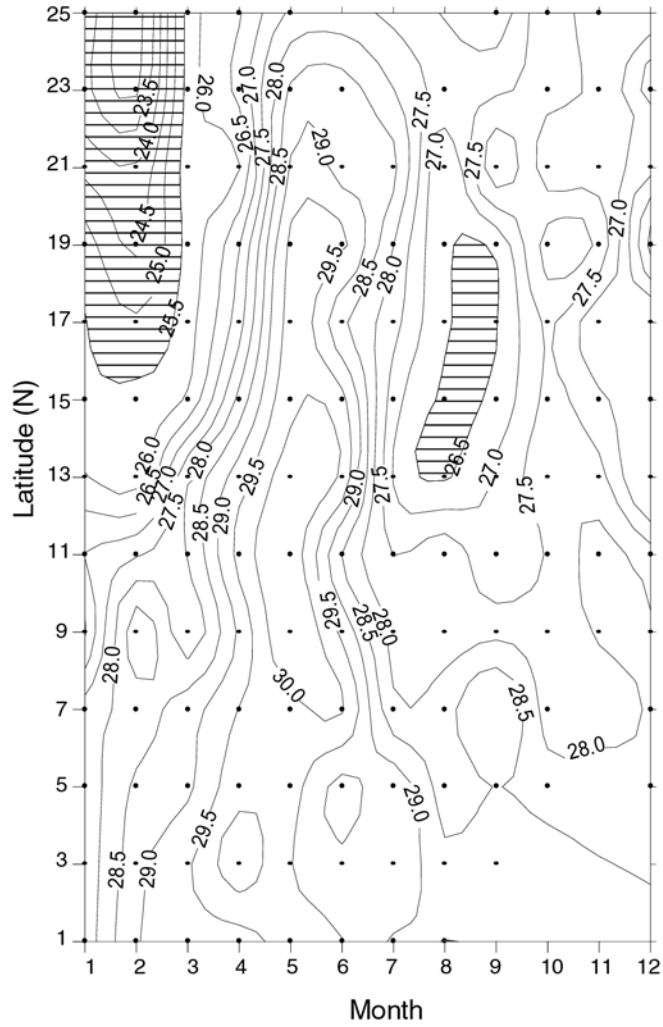


Fig.5 Time-Latitude plot of sea surface temperature (SST, °C) along 64°E. The hatched region indicates SST colder than 25.5°C and 26.5°C during winter and summer respectively.

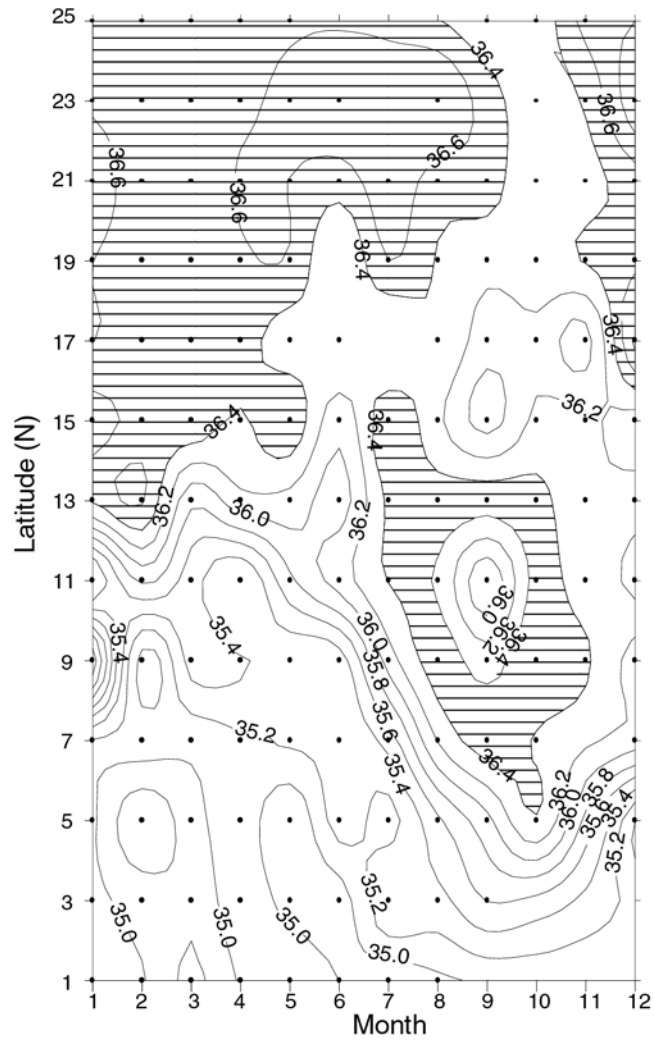


Fig.6 Time-Latitude plot of sea surface salinity (SSS, psu) along 64°E. The hatched region indicates salinity greater than 36.4 psu.



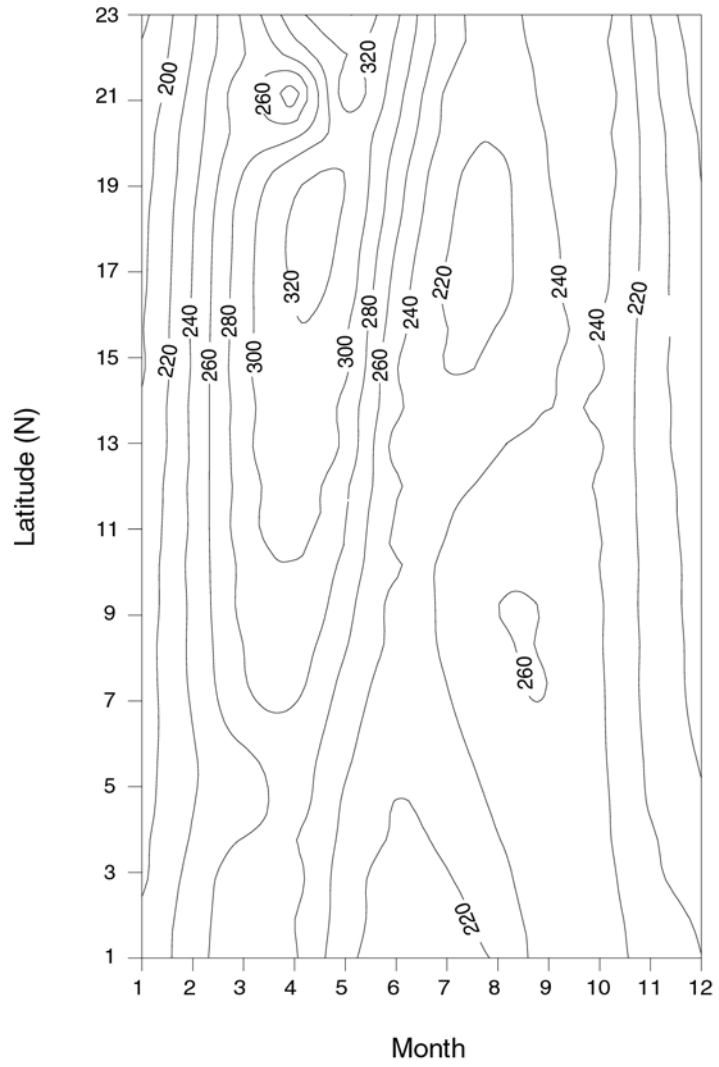


Fig. 7 Time-Latitude plot of short wave radiation (w/m<sup>2</sup>) along 64°E.

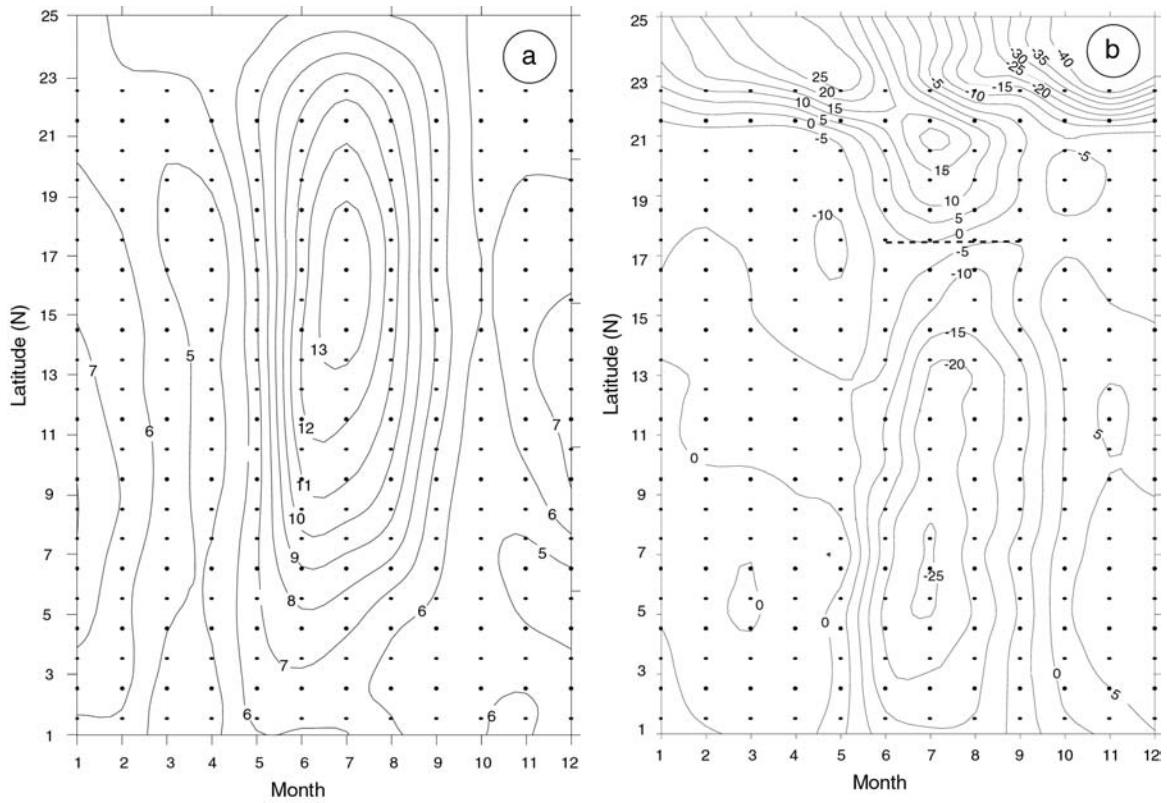


Fig.8 Time-Latitude plot of (a) wind speed (m/s) and (b) wind-stress curl ( $\times 10^{-8}$  pascal  $m^{-1}$ ) along  $64^{\circ}E$ . Broken line at around  $17^{\circ}N$  during June to September represents the mean position of the axis of the Findlater Jet (see text for details).

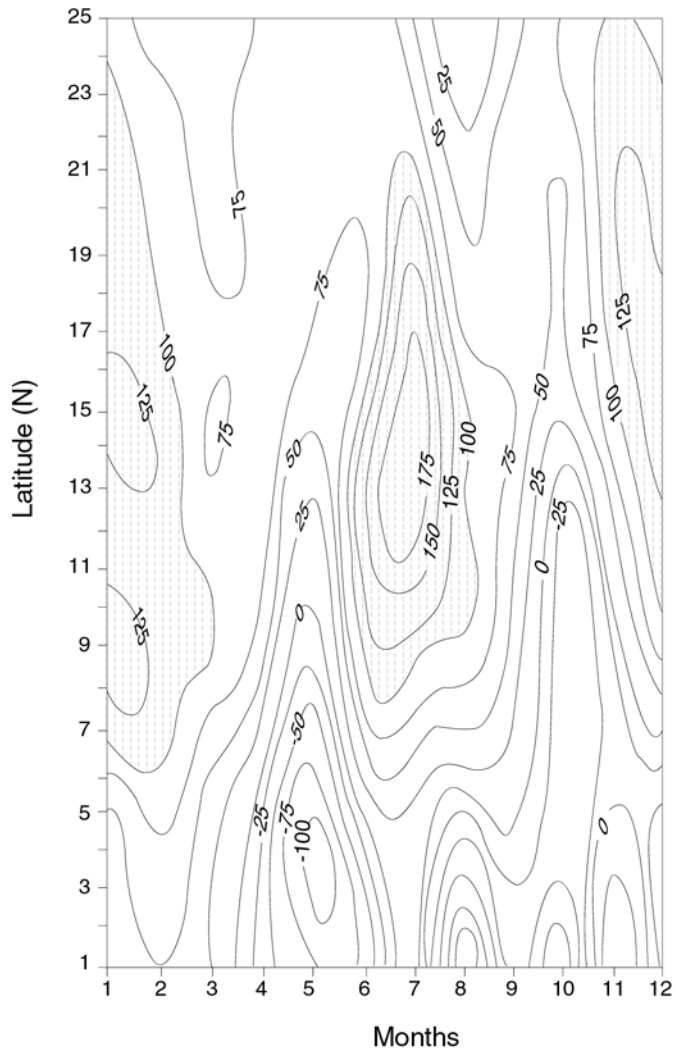


Fig.9 Time-Latitude plot of E-P (mm/month) along 64°E. The stippled region shows where evaporation exceeds precipitation by 100 mm/month.

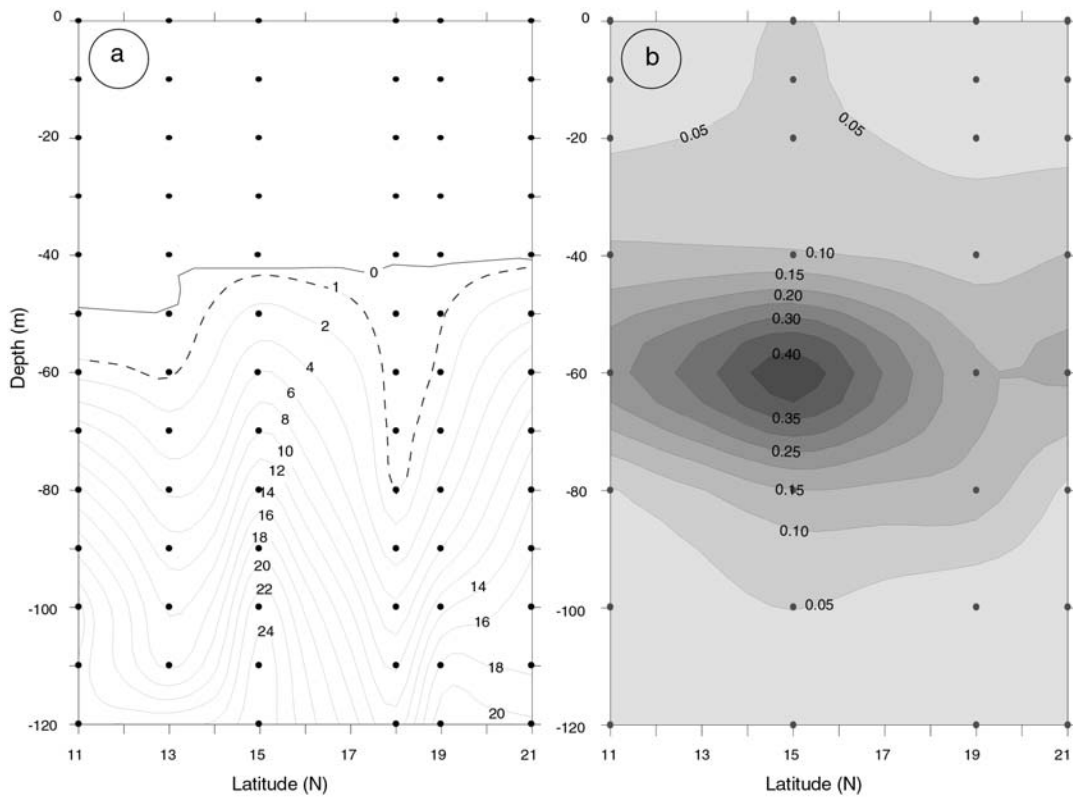


Fig. 10 Vertical section of (a) nitrate ( $\mu\text{M}$ ) and chlorophyll *a* in the upper 120m depth during spring Inter monsoon (April-May 1994).

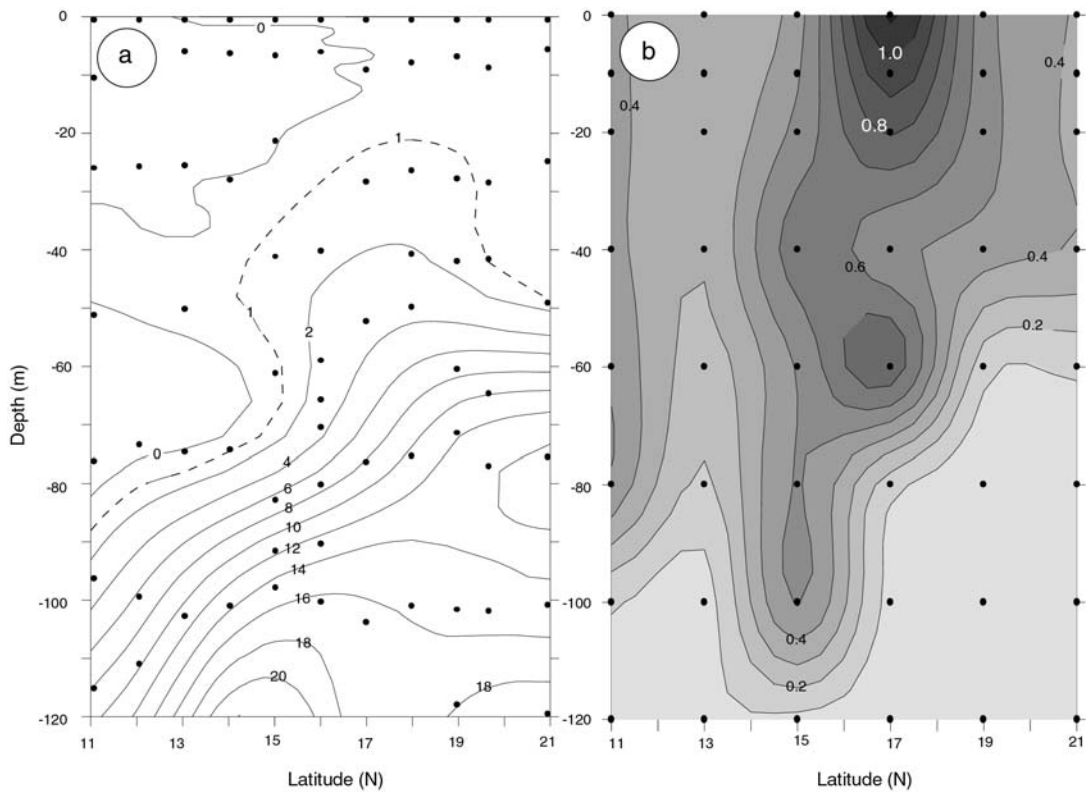


Fig.11 Vertical section of (a) nitrate ( $\mu\text{M}$ ) and chlorophyll *a* in the upper 120m depth during summer monsoon (August 1996). Note that data south of 13°N is from summer (July-August) 1995.

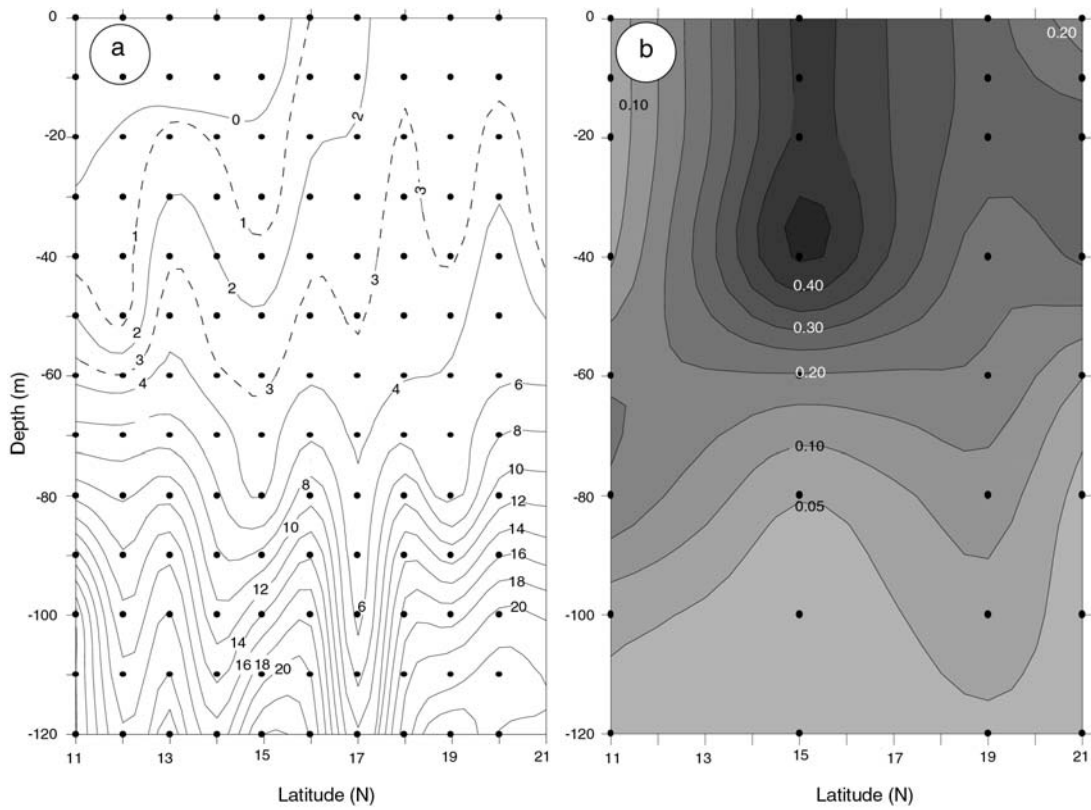


Fig.12 Vertical section of (a) nitrate ( $\mu\text{M}$ ) and chlorophyll *a* in the upper 120m depth during winter monsoon (February-March 1995)

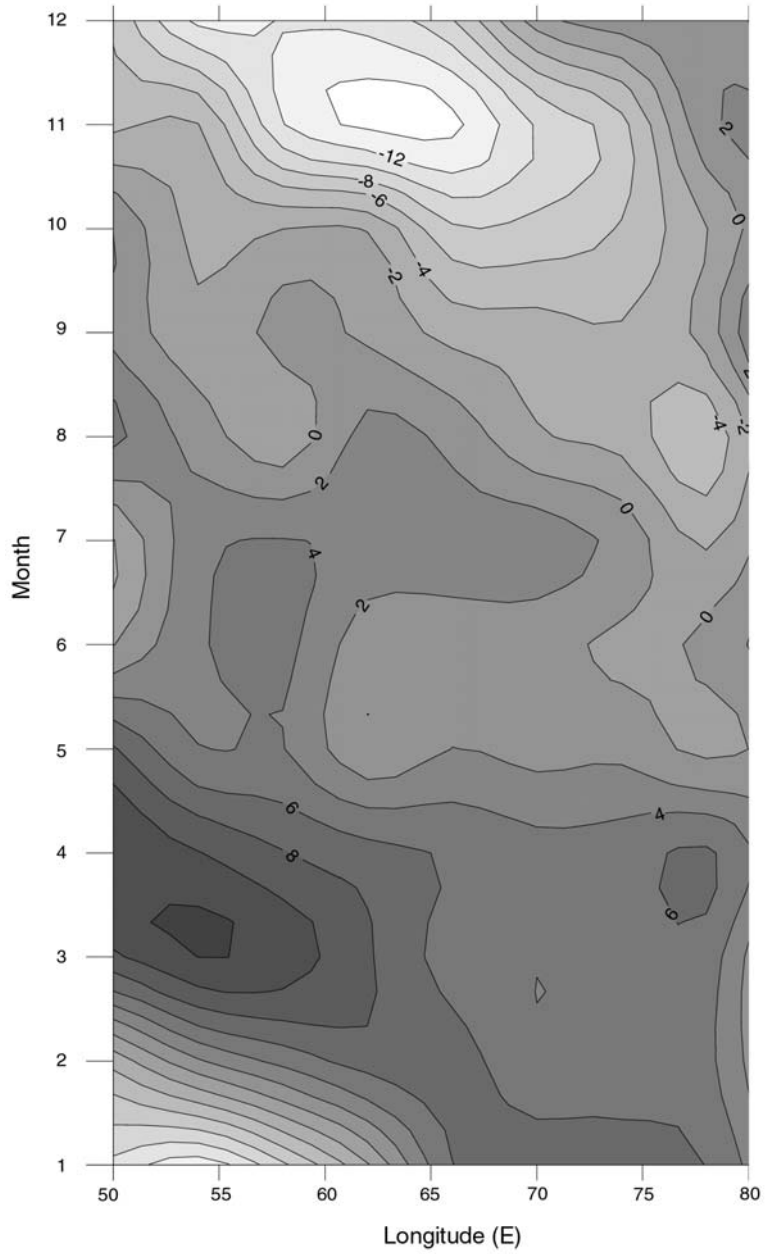


Fig.13 Time-longitude plot of monthly mean (1993-97) SSH anomaly along 5°N. Shaded region indicates high sea level.